Isobaric Analog Resonances in Proton Elastic and Inelastic Scattering from ^{130}Te†

H. R. Hiddleston, C. L. Hollas, V. D. Mistry,* and P. J. Riley
The University of Texas at Austin, Austin, Texas 78712

(Received 1 July 1970)

Proton elastic scattering data are analyzed in the framework of a single-particle theory to obtain energies, partial widths, total widths, and spectroscopic factors for 14 isobaric analog resonances in ^{131}I. Excitation functions and fits are presented and the results are compared with those of similar analyses as well as with those of (d, p) investigations. A total of 42 excited states in ^{130}Te were identified from the inelastic spectra at the various resonances. Groups of states at the $d_{3/2}$, $f_{7/2}$, and $p_{3/2}$ resonances were analyzed as neutron particle–neutron hole states, and fits to the angular-distribution data for these states are presented. The analysis provides proton partial widths, spectroscopic factors, and assignment of possible spins and parities for these states. The ^{130}Te inelastic results are compared with those of other nuclei in the $N=82$ mass region.

I. INTRODUCTION

Elastic and inelastic proton scattering through isobaric analog resonances (IAR) have provided extensive nuclear-structure information. The analysis of proton elastic scattering from ^{130}Te, using the R-matrix theory, has been previously reported.[1] We have used the single-particle model approach of Zaidi and Darmodjo[2] to reanalyze the ^{130}Te elastic scattering data.

There are two essential differences in these methods of analysis. The first involves the method of evaluating the off-resonance background. The previous method relies on a polynominal in the energy to describe the background scattering; the approach used in the present work makes use of an optical potential for this purpose, and thus is believed to be more rigorous. The second difference is concerned with the calculation of the single-particle partial width. The present investigation makes use of an overlap integral based on the Lane model. The rather sensitive radial dependence in the single-particle widths as evaluated by the former method is thus reduced.

The motivation for the reanalysis was twofold. First, it is of interest to compare the results of the present approach with those previously reported, as well as with ^{130}Te(d, p) results.[3] Second, the present investigation has been extended to inelastic scattering, which relies in part upon the parameters determined from the elastic data. Thus, it was thought that the reanalysis would result in a more self-consistent set of nuclear parameters than could otherwise be obtained.

The analysis of inelastic proton scattering through isobaric analog resonances provides spectroscopic information which is not generally available by any other means. That is, to reach many of the same final states accessible with inelastic proton scattering through IAR would require pick-up or stripping reactions on targets of suitable A and Z prepared in various excited states. Inelastic proton scattering to a number of states in the Pb isotopes[4] and, in the mass region of the present work, in ^{142}Nd,[5] ^{140}Ce,[6] ^{138}Ba,[7] and ^{136}Xe,[8] has been successfully described by assuming a single-particle model for the neutron-plus-core system, or parent state. The analog of such a pure parent state may then be represented as resulting from application of the isospin lowering operator:

$$T^- |nC\rangle \rightarrow \left(\frac{1}{2T_0+1}\right)^{1/2} [\,|pC\rangle + (2T_0)^{1/2}|nA\rangle]\,,$$

where $|nC\rangle$, $|pC\rangle$, and $|nA\rangle$ represent the configurations for neutron plus core, proton plus core, and neutron plus the analog of the core, respectively.

Inelastic proton decay of the IAR of the nuclei mentioned above was found to populate preferentially states with a neutron particle-neutron hole configuration which arise from the $|nA\rangle$ term above. For the generalized case of a parent state which contains, in addition to the $|nC\rangle$ part, terms consisting of a neutron coupled to excited states of the core, application of the T^- operator will now yield $|pC^*\rangle$ and $|nA^*\rangle$ terms:

$$T^-\Big(\alpha|nC\rangle + \sum_{I,j}\beta_{Ij}|n_jC_I^*\rangle\Big) \rightarrow \left(\frac{1}{2T_0+1}\right)^{1/2}\Big[\Big(\alpha|pC\rangle + \sum_{I,j}\beta_{Ij}|p_jC_I^*\rangle\Big) + (2T_0)^{1/2}\Big(\alpha|nA\rangle + \sum_{I,j}\beta_{Ij}|n_jA_I^*\rangle\Big)\Big]_J\,.$$

Here J is the spin of the analog state and I is the spin of the excited core or analog of the core. The sum extends over all values of j consistent with the coupling to spin J of j with each spin I of the excited state of the core or analog of the core. The α^2 and the β_{Ij}^2 are the spectroscopic factors and are such that to preserve normalization,

$$\alpha^2 + \sum_{I,j} \beta_{Ij}{}^2 = 1 .$$

The analog state is formed through the $|pC\rangle$ channel but may decay through the $|pC\rangle$, $|pC^*\rangle$, $|nA\rangle$, or $|nA^*\rangle$ channels. Decay of IAR in ^{131}I through the $|pC^*\rangle$ configuration has been discussed in earlier papers.[9,10] The present analysis of the decay through the $|pC\rangle$ channel (elastic scattering) makes available new resonance parameters. In addition, we report on and discuss here neutron particle-hole states observed through decay of the IAR into the $|nA\rangle$ and $|nA^*\rangle$ channels resulting from inelastic data taken at the $d_{3/2}$, $s_{1/2}$, $f_{7/2}$, and second $p_{3/2}$ IAR in ^{131}I at energies of 7.978, 8.282, 10.209, and 10.500 MeV, respectively.

II. ELASTIC ANALYSIS

A. Theory

Using the energy-averaged S matrix of Zaidi and Dyer,[11] we may rewrite for proton elastic scattering from spin-zero targets in channel λ:

$$S_{\lambda\lambda} = e^{2i\delta_\lambda}\left[\left|\frac{1 - Y_\lambda + 2i(\Delta/\Gamma_{sp})Y_\lambda}{1 + Y_\lambda + 2i(\Delta/\Gamma_{sp})Y_\lambda}\right| - ie^{-i(\phi_\lambda + \chi_\lambda)}\frac{S_{pp}\Gamma_{sp}|a_{\lambda\lambda}|^{-2}}{E - E_R + i\Gamma/2}\right]e^{-i(\phi_\lambda - \chi_\lambda)} .$$

E_R is the resonance energy, Γ is the total width, and δ_λ is the optical-model phase shift. $a_{\lambda\lambda}$ is the width damping factor due to the background of $T^<$ states and is given by

$$|a_{\lambda\lambda}|^2 = |1 + Y_\lambda + 2i(\Delta/\Gamma_{sp})Y_\lambda|^2 .$$

The phases φ_λ and χ_λ, as well as the single-particle shift Δ, are defined in Ref. 11.

The code JULIUS[2,12] was used to generate theoretical elastic scattering excitation functions, using the above expressions for the scattering matrix. The quantity $S_{pp}\Gamma_{sp}|a_{\lambda\lambda}|^{-2}$, which we define as $\tilde{\Gamma}_p$, is the experimental partial width of the analog resonance to be obtained from the fitting. S_{pp} is the elastic spectroscopic factor and Γ_{sp} is the theoretical single-particle partial width for an isolated analog state for which only the elastic proton channel is open. It is evaluated from the expression

$$\Gamma_{sp} = (kT_0/E)\,|\langle \chi_{pC}^{(+)}|\, V_1 |\varphi_{nA}\rangle|^2$$

by the use of code GPMAIN.[12] The radial wave functions $\chi_{pC}^{(+)}$ and ϕ_{nA} are obtained by solution of the homogeneous Lane equations and the $\chi_{pC}^{(+)}$ wave function is normalized to a δ function in the energy E. The strength of the phenomenological symmetry potential V_1 is fixed by the emperical relation,

$$\tfrac{1}{2}T_0 V_1 = 26(N - Z)/A ,$$

and is taken to be a Woods-Saxon potential with the same geometry as the real central potentials in the pC and nA channels. The quantity $\Gamma_{sp}|a_{\lambda\lambda}|^{-2}$, which we write as $\tilde{\Gamma}_{sp}$, corresponds to the partial width of an analog resonance with a spectroscopic factor of unity. In terms of the Y_λ,

$$\tilde{\Gamma}_{sp} = \Gamma_{sp}|a_{\lambda\lambda}|^{-2} = \Gamma_{sp}\frac{1}{1 + 2Y_\lambda + Y_\lambda{}^2(1 + 4\Delta^2/\Gamma_{sp}{}^2)} .$$

The product $S_{pp}\Gamma_{sp}$, often called Γ_p, is a reduced partial width; that is, the partial width that an analog state would have in the absence of background absorption. The elastic spectroscopic factor then may be written as

$$S_{pp} = \tilde{\Gamma}_p/\tilde{\Gamma}_{sp} = \Gamma_p/\Gamma_{sp} .$$

Although both quantities have been used in the literature, $\tilde{\Gamma}_p$, rather than Γ_p, must be used for comparison of partial widths with those extracted by other methods of resonance analysis, or for subsequent inelastic cross-section calculations. This distinction can be especially important for cases where values of Y_λ, which are related to the penetrability, are significantly greater than zero.

In the extraction of resonance and optical parameters, the efforts at fitting are first concentrated on the off-resonance regions, since this allows the determination of the Y_λ. That is, the S matrix reduces to a single term,

$$S = |S_{\lambda\lambda}|_1 = \left|\frac{1 - Y_\lambda + 2i(\Delta/\Gamma_{sp})Y_\lambda}{1 + Y_\lambda + 2i(\Delta/\Gamma_{sp})Y_\lambda}\right| ,$$

which can be solved for Y_λ:

$$Y_\lambda = \frac{(S^2 + 1) - 2[S^2 - (S^2 - 1)^2(\Delta/\Gamma_{sp})^2]^{1/2}}{(1 - S^2)[1 + 4(\Delta/\Gamma_{sp})^2]} .$$

$\tilde{\Gamma}_{sp}$ and the other quantities expressed in terms of the Y_λ are put back into the full S matrix, and the resonance regions are then fitted by varying the resonance parameters E_R, S_{pp}, and Γ.

In the present analysis Δ was also treated as a free parameter. For all but the $f_{7/2}$ IAR at 10.209 MeV, good fits were obtained with negligibly small values of Δ. In all cases, $(\Delta/\Gamma_{sp})^2 Y_\lambda{}^2 \ll 1$. Thus, $\tilde{\Gamma}_p = f\Gamma_p \cong [1/(1 + 2Y_\lambda)]\Gamma_p$, where we have defined f as $|a_{\lambda\lambda}|^{-2}$ and have kept the first two terms in the expansion of f in terms of the Y_λ; i.e., $f \cong 1/(1 + 2Y_\lambda)$. In our analysis $0 \leq Y_\lambda < 1$. Consequently, $f \leq 1$ and $\tilde{\Gamma}_p \leq \Gamma_p$ as expected, since the observed width $\tilde{\Gamma}_p$ results from the inclusion of the effects of the mixing of the analog state with the surrounding $T^<$ states.

B. Optical and Resonance Parameters

The optical potential utilized by the elastic scat-

TABLE I. Optical-model parameters for proton elastic scattering from ^{130}Te. Results of this work using a surface-peaked imaginary term and an energy-dependent real-well depth.

	JULIUS parameters	
(MeV)	(F)	(F)
$V_S = (63.0 - 0.5E)$	$r_1 = 1.22$	$a_1 = 0.67$
$W' = 11.0$	$r_3 = 1.23$	$a_3 = 0.67$
$V_{so} = 7.50$	$r_4 = 1.22$	$a_4 = 0.67$
	$r_c = 1.25$	

TABLE II. Optical-model parameters for proton elastic scattering from ^{130}Te. Results of Ref. 1 using both surface and volume absorption terms. The notation follows that of Ref. 1.

	OPTIX I parameters	
(MeV)	(F)	(F)
$V_S = 58.7$	$r_1 = 1.22$	$a_1 = 0.65$
$W = 3.50$	$r_2 = 1.22$	$a_2 = 0.65$
$W' = 6.00$	$r_3 = 1.22$	$a_3 = 0.65$
$V_{so} = 7.50$	$r_4 = 1.10$	$a_4 = 0.65$
	$r_c = 1.22$	

tering code JULIUS contains a surface-peaked imaginary part and a real spin-orbit part. It is of a Woods-Saxon type and is given by the following expression:

$$V(J, l, r) = -V_S f_1 - 4a_3 i W' \frac{d}{dr}(f_3) \quad \text{Central}$$

$$+\vec{\sigma}\cdot\vec{l}\left(\frac{\hbar^2}{m_\pi c}\right)^2 \frac{V_{so}}{r}\frac{d}{dr}(f_4) \quad \text{Spin-orbit}$$

$$+\frac{Ze^2}{2R_C}\left(3 - \frac{r^2}{R_C^2}\right), \quad r \leq R_C$$

or Coulomb

$$+Ze^2/r, \quad r > R_C,$$

where

$$f_i = f(r, R_i, a_i) = [1 + e^{(r-R_i)/a_i}]^{-1}$$

and

$$R_i = r_i A^{1/3}.$$

This potential does not include the volume absorption term $-iWf_2$ used by Foster, Riley, and Moore,[1] in fits to off-resonance angular-distribution data.

The optical parameters determined in the present work are in good agreement with those obtained previously by Foster, Riley, and Moore,[1] as can be seen in Tables I and II. An energy-dependent real-well depth was used in the present work, since it resulted in slightly improved fits. Over the energy range fitted, V_s varied from 59.1 to 57.0 MeV, in good agreement with Foster's value of 58.7 MeV.

The data and fits obtained in the present work for proton elastic scattering from ^{130}Te are shown in

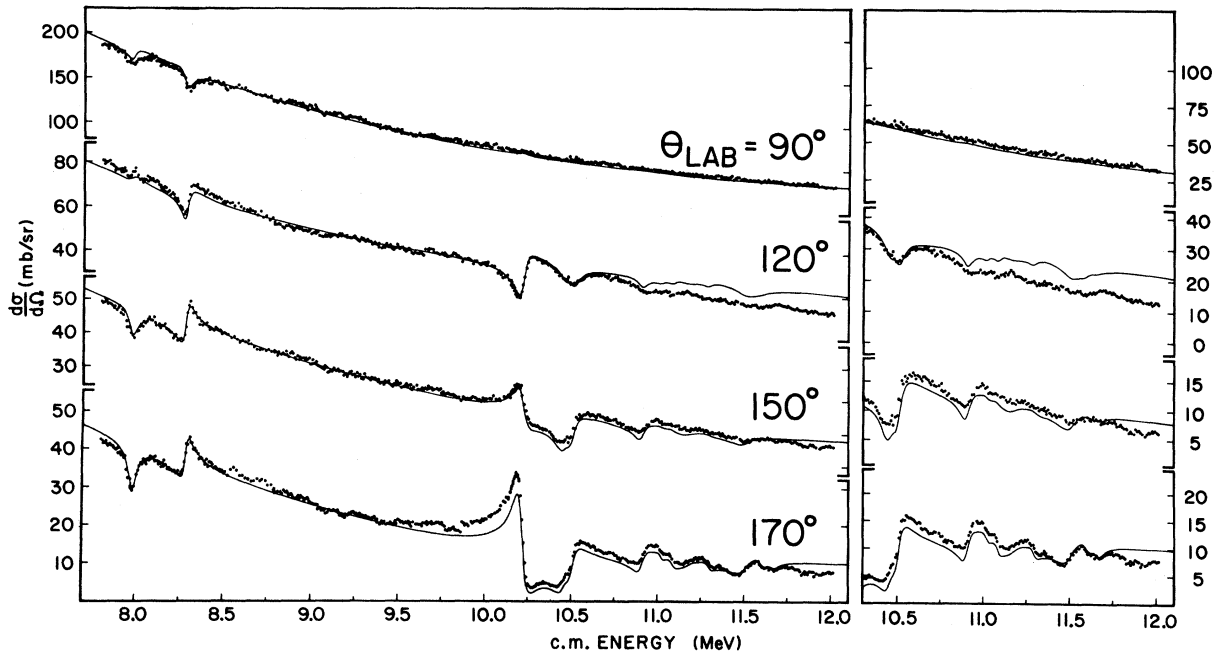

FIG. 1. Complete c.m. excitation functions for proton elastic scattering from ^{130}Te from 7.80 to 12.0 MeV and laboratory angles of 90, 120, 150, and 170°. The data are that of Ref. 1, whereas the fits are from the analysis presented in this work. The region from 10.3 to 12.0 MeV is shown scaled up by a factor of 1.5 to clarify the detail at the higher energies.

TABLE III. The c.m. resonance energies, L values, probable J values, and partial widths for elastic proton scattering from ^{130}Te. The partial widths from two other analyses are included for comparison. The correction factor for absorption due to the $T^<$ states is tabulated as f. The values in parentheses are in some doubt.

E_R (MeV)	L_J	f	$\tilde{\Gamma}_p$ (keV)	Γ_p (keV) (Ref. 1)	Γ_p (keV) (Ref. 9)
7.798	$d_{3/2}$	0.89	5.9	8.5	4.1
8.282	$s_{1/2}$	0.72	9.1	10.2	11.1
10.209	$f_{7/2}$	0.85	18.2	18.4	15.8
10.453	$p_{3/2}$	0.67	8.7	3.2	5.0
10.500	$p_{3/2}$	0.61	14.9	14.7	8.8
10.905	$p_{1/2}$	0.63	15.4	18.9	19
11.020	$f_{5/2}$	0.79	0.8	(0.6)	
11.085	$f_{5/2}$	0.79	1.6		2.7 [a]
11.170	$p_{1/2}$	0.62	3.7		
11.295	$f_{5/2}$	0.78	1.3		2 [a]
11.505	$p_{1/2}$	0.61	(23.2)		7.6
11.597	$f_{5/2}$	0.76	2.3		
11.660	$f_{5/2}$	0.75	1.0		
11.680	$p_{1/2}$	0.59	3.3		

[a] L_J of $f_{7/2}$ assigned to these levels.

Fig. 1. The resonance parameters for the 14 resonances identified in this analysis are listed in Table III. We have included the values for f as well as for $\tilde{\Gamma}_p$. It is apparent that Y_λ depends on the l value of the resonance, resulting in a smaller value of f and thus a greater percentage difference in Γ_p and $\tilde{\Gamma}_p$ for the lower partial waves as expected. We show also, for comparison, partial widths obtained in the analysis of Ref. 1, and partial widths taken from the recent work of Burde *et al.*[9] In most cases, there is good over-all agreement between the above partial widths and the values of $\tilde{\Gamma}_p$ obtained in the present work.

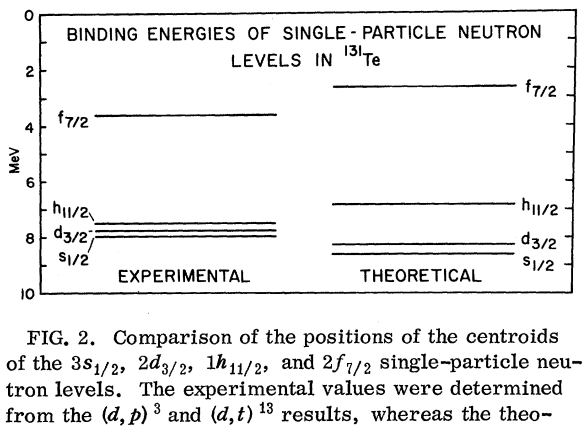

FIG. 2. Comparison of the positions of the centroids of the $3s_{1/2}$, $2d_{3/2}$, $1h_{11/2}$, and $2f_{7/2}$ single-particle neutron levels. The experimental values were determined from the (d,p) [3] and (d,t) [13] results, whereas the theoretical values are those necessary to bind a single neutron at the appropriate level in the potential described in the text.

C. Theoretical Partial Widths and Spectroscopic Factors

Code GPMAIN was used to calculate the bound-state wave functions of the various single-particle neutron levels in ^{131}Te and the single-particle partial widths for elastic proton scattering. Code GPMAIN uses the same potential geometry (radius and diffuseness) as does JULIUS except that only the spin-orbit and real central terms are employed, and no imaginary well is used. It was possible to find a single potential which reproduced reasonably well the binding energies of the first four single-particle neutron levels in ^{131}Te. The well depth used was 47.3 MeV, in excellent agreement with the real proton well depth after subtraction of the symmetry potential term, T_0V_1. The binding energies deduced using this potential are shown compared in Fig. 2 with the "experimental" binding energies, calculated from the results of (d,p),[3] and (d,t) [13] work.

The deduced spectroscopic factors are shown in Table IV, together with the spectroscopic factors of Ref. 1 and the (d,p) assignments of Graue *et al.*[3] In addition, the deduced spectroscopic factors of Burde *et al.*[9] are given. The method of analysis of Burde *et al.*[9] is similar to that employed in Ref. 1. Over-all, the spectroscopic factors of the four analyses are in good agreement, with some notable exceptions. The spectroscopic factor of the first state ($\frac{3}{2}^+$), $S_{pp}=0.48$, in the present work, is nearly a factor of 2 larger than the spectroscopic factors for the same state obtained in the other three analyses, although the ratios of Γ_p/Γ for this resonance are all comparable. Similarly, the spectroscopic factor of the second state ($\frac{1}{2}^+$) of $S_{pp}=0.10$ obtained in the work of Ref. 1 is notably low. There is excellent over-all agreement in the value of the spectroscopic factor ($S\cong 0.50$) of the first $\frac{7}{2}^-$, $l=3$ state.

There is some disagreement in the spectroscopic factors for the first two rather closely spaced $\frac{3}{2}^-$ states observed at approximately 10.5 MeV in the elastic scattering data. The spectroscopic factors for these two states obtained in the present work are approximately a factor of 2 greater than the values obtained in the work of Burde *et al.*[9] The value given in Ref. 1 for the first of these states agrees with that of Burde *et al.*[9]; the value for the second state is in agreement with the present study. The (d,p) work of Graue *et al.*[3] gives tentative spectroscopic factors of 0.06 and 0.22, respectively, for the parent analogs of these two states, in reasonable agreement with available elastic data. Some disagreement in the spectroscopic factors deduced from the elastic scattering analyses can be expected, especially when several

TABLE IV. Summary of resonance parameters from analyses of elastic proton scattering from ^{130}Te and comparison with the results of ^{130}Te(d,p) work.

(p,p_0) (This work)						(p,p_0) (Ref. 1)						(p,p) (Ref. 9)						(d,p) (Ref. 3)			
E_R (MeV)	l	J^π	$\tilde{\Gamma}_p$ (keV)	Γ (keV)	S_{pp}	E_R (MeV)	l	J^π	Γ_p (keV)	Γ (keV)	S_{pp}	E_R (MeV)	l	J^π	Γ_p (keV)	Γ (keV)	S_{pp}	E_{EXC} (MeV)	l	J^π	S_{dp}
7.978	2	$\frac{3}{2}^+$	5.9	60	0.48	7.977	2	$\frac{3}{2}^+$	8.5	77	0.26	7.970	2	$\frac{3}{2}^+$	4.12	50	0.24	0.0	2	$\frac{3}{2}^+$	0.25
																		0.183	5	$\frac{11}{2}^-$	0.17
8.282	0	$\frac{1}{2}^+$	9.1	50	0.23	8.282	0	$\frac{1}{2}^+$	10.2	60	0.10	8.272	0	$\frac{1}{2}^+$	11.1	55	0.21	0.297	0	$\frac{1}{2}^+$	0.16
																		0.882	1	$\frac{3}{2}^-$	0.0045
																		1.043	0	$\frac{1}{2}^+$	0.005
						(9.18)												1.209	2	$(\frac{5}{2}^+)$	(0.02)
						(9.44)												1.471	1	$(\frac{3}{2}^-)$	(0.005)
																		1.722	(1)	$(\frac{3}{2}^-)$	(0.004)
						(9.75)												1.786	1	$(\frac{3}{2}^-)$	(0.009)
																		2.014	1	$(\frac{3}{2}^-)$	(0.003)
																		2.092	1	$(\frac{3}{2}^-)$	(0.003)
10.209	3	$\frac{7}{2}^-$	18.2	75	0.50	10.209	3	$\frac{7}{2}^-$	18.4	78	0.49	10.200	3	$\frac{7}{2}^-$	15.8	79	0.45	2.278	3	$\frac{7}{2}^-$	0.50
																		2.329	(1)	$(\frac{3}{2}^-)$	(0.070)
																		2.372	(1)	$(\frac{3}{2}^-)$	(0.009)
10.458	1	$\frac{3}{2}^-$	8.7	70	0.11	10.437	1	$\frac{3}{2}^-$	3.2	45	0.04	10.455	1	$\frac{3}{2}^-$	5.0	61	0.054	2.512	1	$(\frac{3}{2}^-)$	(0.060)
10.500	1	$\frac{3}{2}^-$	14.9	80	0.21	10.496	1	$\frac{3}{2}^-$	14.7	79	0.20	10.520	1	$\frac{3}{2}^-$	8.8	63	0.093	2.581	1	$(\frac{3}{2}^-)$	(0.22)
																		2.752	1	$(\frac{3}{2}^-)$	(0.008)
10.905	1	$\frac{1}{2}^-$	15.4	75	0.20	10.895	1	$\frac{1}{2}^-$	18.9	103	0.20	10.915	1	$\frac{1}{2}^-$	19	120	0.182	3.002	1	$(\frac{1}{2}^-)$	(0.095)
11.020	3	$(\frac{5}{2}^-)$	0.8	40	(0.015)	11.007	(3)	$(\frac{5}{2}^-)$	(0.6)	(46)	(0.01)							3.141	(3)	$(\frac{7}{2}^-)$	(0.03)
11.085	3	$(\frac{5}{2}^-)$	1.6	55	(0.028)	11.07	3	$(\frac{5}{2}^-)$				11.120	(3)	$(\frac{7}{2}^-)$	2.7	100	0.052	3.183	(3)	$(\frac{7}{2}^-)$	(0.04)
11.170	1	$(\frac{1}{2}^-)$	3.7	90	(0.05)													(3.203)			
11.295	3	$(\frac{5}{2}^-)$	1.3	50	(0.023)							11.290	3	$(\frac{7}{2}^-)$	2	80	0.036	3.353	3	$(\frac{7}{2}^-)$	(0.02)
11.505	(1)	$(\frac{1}{2}^-)$	(23.2)	(140)	(0.33)	11.46	(1)					11.490	1	$(\frac{1}{2}^-)$	7.6	71	0.064	3.600	(1)	$(\frac{1}{2}^-)$	(0.030)
11.597	3	$(\frac{5}{2}^-)$	2.3	75	(0.04)	11.59	(3)					11.590	(3)					3.621	(1)	$(\frac{1}{2}^-)$	(0.024)
11.660	3	$(\frac{5}{2}^-)$	1.0	50	(0.017)	11.66	(1)											3.663	(2)	$(\frac{5}{2}^+)$	(0.032)
11.680	1	$(\frac{1}{2}^-)$	3.3	100	(0.05)													3.686	1	$(\frac{1}{2}^-)$	(0.055)
						11.92	(1)											3.706	(2)	$(\frac{5}{2}^+)$	(0.041)

resonances are rather close together, because of differences in the methods used to describe the background scattering. The unusually large values for the partial width, total width, and resulting spectroscopic factor for the $p_{1/2}$ IAR at 11.505 MeV are included in parentheses since at this energy the data and the theoretical fit exhibit a crossover at 170°. The fits at the other angles do not reflect such large widths for this resonance, nor is a large $p_{1/2}$ state evident in the (d,p) work near the corresponding excitation energy.

Over-all, the present analysis tends to give rather large spectroscopic factors, particularly for low orbital angular momentum transfer values. Other than the ambiguity associated with the extraction of partial widths for overlapping resonances, additional discrepancy is clearly associated with the method of extraction of Γ_{sp}. At higher energies, where the level spacings approach the resonant widths, the determination of the partial widths, and consequently the spectroscopic factors, becomes uncertain in all elastic analyses.

III. INELASTIC ANALYSIS

A. Introduction

Neutron particle-hole states in ^{130}Te, populated by inelastic proton emission of a $2d_{3/2}$ or $3s_{1/2}$ proton at the $f_{7/2}$ IAR, have been previously reported.[14] These states are easily observed since the $f_{7/2}$ IAR in ^{131}I has a rather large spectroscopic factor, and the $d_{3/2}$ and $s_{1/2}$ subshells in ^{130}Te are relatively full. Figure 3 shows the excitation functions from 10.15 to 10.75 MeV for elastic and inelastic scattering of protons from ^{130}Te. The sharp resonance in the group of states at excitations from 4.366 to 4.496 MeV at the energy of the $f_{7/2}$ IAR indicates that these states are neutron particle-hole states in ^{130}Te, with the particle in the $f_{7/2}$ level. The preliminary analysis of six of these states was reported in Ref. 14.

New inelastic data were taken at the $f_{7/2}$ IAR in ^{131}I at 10.209 MeV and exhibit a much better peak-to-background ratio and better resolution than that of the previous work; and since, in addition, the present analysis provides new elastic resonance parameters, the neutron particle-hole states observed were reanalyzed. New inelastic data were also taken at the $d_{3/2}$, $s_{1/2}$, and second $p_{3/2}$ IAR at 7.978, 8.282, and 10.500 MeV, respectively. The second $p_{3/2}$ IAR was chosen, since it has a significantly larger spectroscopic factor than the first $p_{3/2}$ IAR at 10.453 MeV. Both at the $d_{3/2}$ and at the second $p_{3/2}$ IAR, states whose behavior is consistent with their identification as neutron particle-hole states were observed. Consequently, the inelastic analysis was extended to include all states identified as particle hole in nature.

B. Experimental Procedure

The proton beam was obtained from the University of Texas EN tandem Van de Graaff accelerator. The targets were fabricated by vacuum evaporation of 99.9% isotopically enriched ^{130}Te onto thin carbon backings (~10 μg/cm^2). The target thicknesses were typically between 100 and 300 μg/cm^2 and were determined by the elastic scattering, assumed to be purely Rutherford, of from 3- to 4-MeV protons.

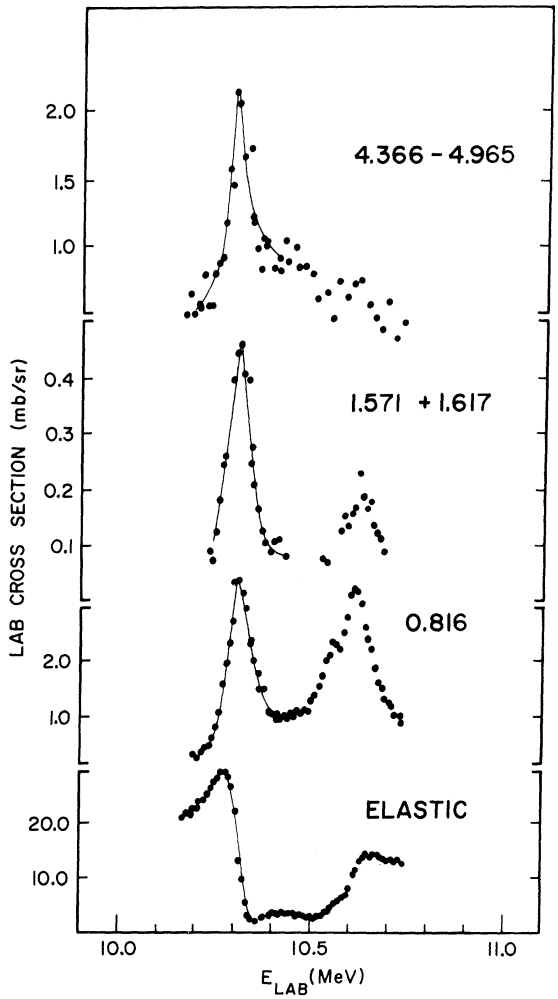

FIG. 3. Laboratory excitation functions at 170° for proton scattering from ^{130}Te from 10.15 to 10.75 MeV. The elastic and first 2^+ state at 0.816 MeV are shown, as well as the sums of the yields of the 1.571 + 1.617-MeV doublet and of a group of states from 4.366- to 4.965-MeV excitation. The latter group is subsequently identified as arising from neutron particle-hole states in ^{130}Te. The three resonances evident in the elastic and 2^+ curves correspond to the 10.209-MeV $f_{7/2}$, 10.458-MeV $p_{3/2}$, and 10.500-MeV $p_{3/2}$ IAR.

Most of the data were taken in a 40-in.-diam scattering chamber; for some of the mearurements, however, a 20-in.-diam chamber was used. In all cases, 2-mm-thick lithium-drifted silicon detectors cooled to dry-ice temperature were used. Improved preamplifiers, more thorough detector shielding, and a better beam focus are believed to be chiefly responsible for the improved peak-to-background ratio of this data over that of the earlier work.[14] The data taken at each IAR consist of angular distributions, mostly at backward angles, at the energy of the analog resonance. Each resonance was located by taking excitation function measurements in 10-keV steps in the neighborhood of the elastic resonance, and searching for a maximum in the yield to the 2^+ collective, first excited state in ^{130}Te at an excitation of 0.816 MeV. The absolute inelastic cross sections are very sensitive to the determination of this maximum and thus may be accurate to only 10–15%, but the relative errors are expected to be less.

The inelastic data analyzed in the present work at the $d_{3/2}$ resonance (7.978 MeV) consist of angular distributions from 70 to 170 in 10° steps for eight states ranging from 2.173 to 2.674 MeV in excitation. The angular distributions at the $f_{7/2}$ resonance (10.209 MeV) were taken from 50 to 160° for nine states with excitation energies from 4.366 to 4.496 MeV. The data at the $p_{3/2}$ resonance (10.500 MeV) consist of angular distributions from 80 to 170° in 10° steps for two strong states at 4.778- and 4.838-MeV excitation. No angular-distribution data are presented for the $s_{1/2}$ resonance (8.282 MeV), since no state or group of states was observed in the spectra with the approximate expected excitation energy for neutron particle-hole states.

C. Energy Levels and Spectra

Typical on- and off-resonance spectra at the

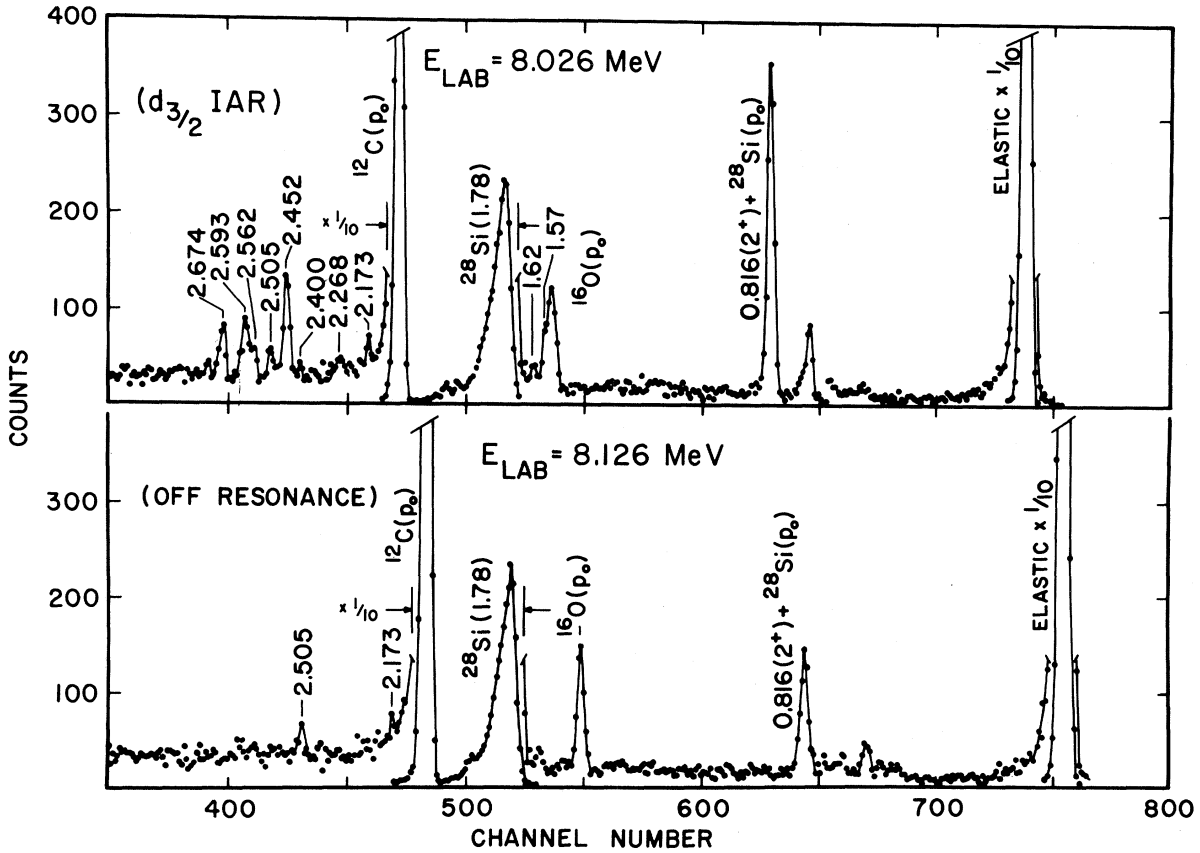

FIG. 4. Pulse-height spectra for the inelastic scattering of protons from ^{130}Te at a scattering angle of 170°. The upper spectrum was taken at a laboratory energy of 8.026 MeV which corresponds to the $d_{3/2}$ IAR at 7.978 MeV, whereas the lower spectrum was taken 100 keV above the resonance. The accumulated charge for each spectrum was 1000 μC. The excitation energies indicated are for states in ^{130}Te. The group of states appearing in the on-resonance spectrum at excitation energies from 2.2 to 2.6 MeV are subsequently identified as neutron particle-hole states. The broad peak identified as the 1.78-MeV state in ^{28}Si arises from inelastic scattering in the detector of protons from the ^{130}Te elastic peak.

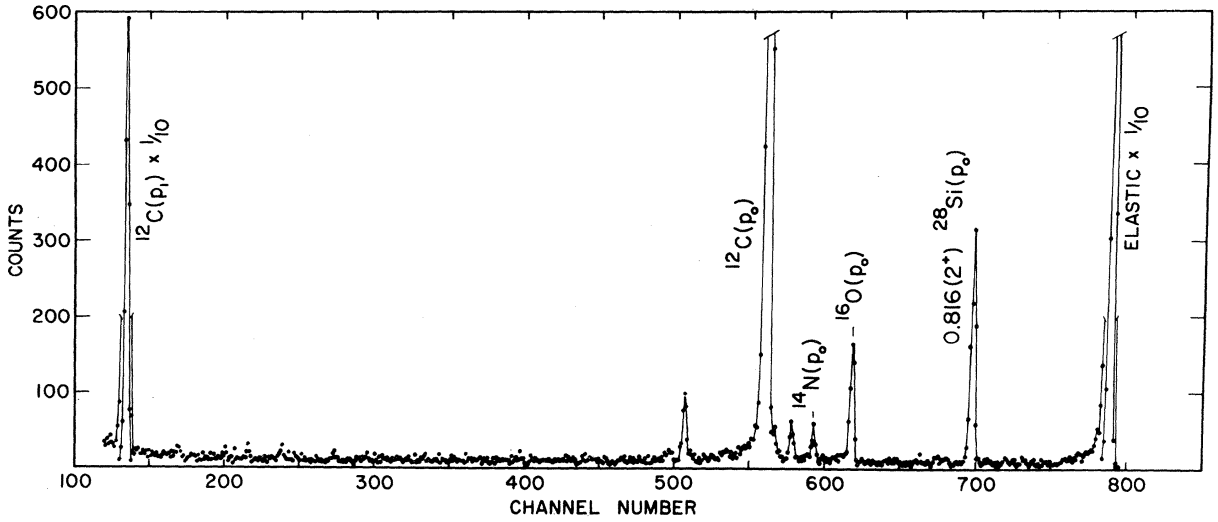

FIG. 5. Pulse-height spectrum for the inelastic scattering of protons from ^{130}Te at a scattering angle of 150° and a laboratory energy of 8.281 MeV which corresponds to the $s_{1/2}$ IAR. The target is the same as for the spectra of Fig. 4 and the charge accumulated is 500 μC. No resonating states are observed at the expected excitation energies, from 2.8 to 3.0 MeV, for formation of neutron particle-hole states.

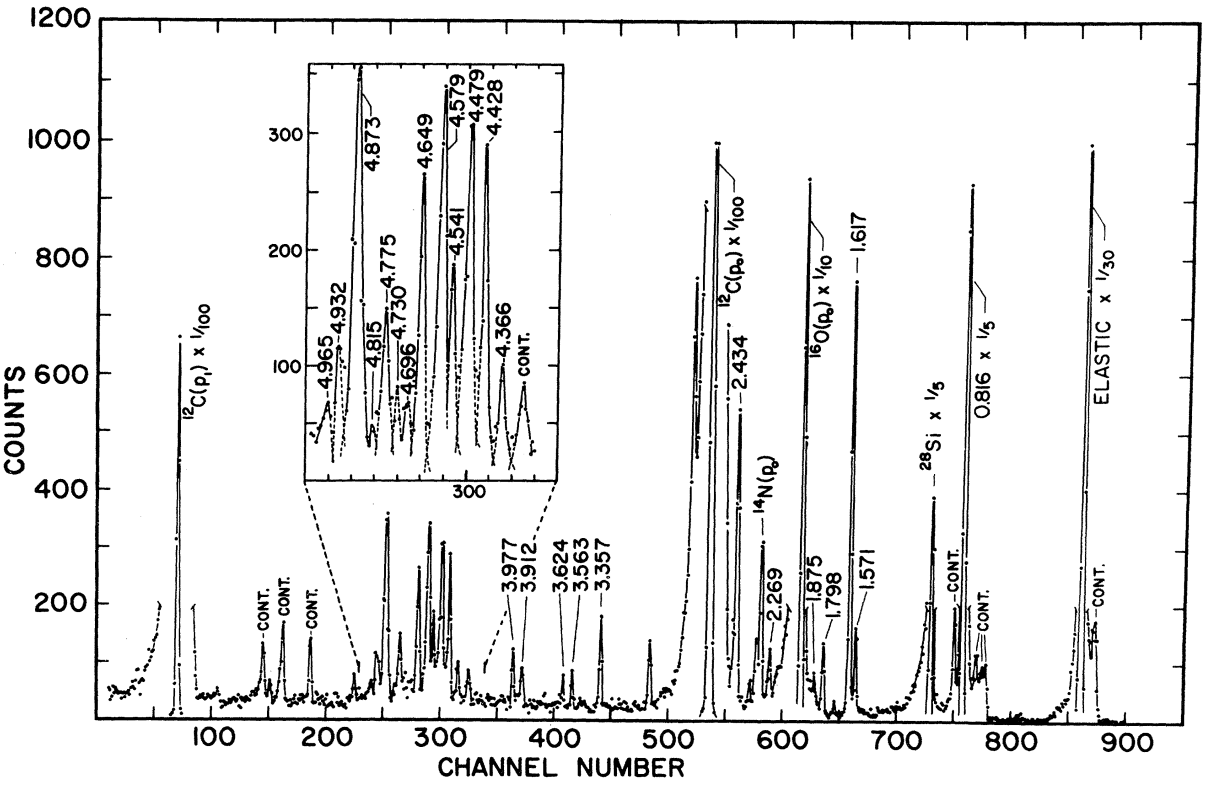

FIG. 6. Pulse-height spectrum for the inelastic scattering of protons from ^{130}Te at a scattering angle of 160° and a laboratory proton energy of 10.296 MeV which corresponds to the $f_{7/2}$ IAR at 10.209 MeV. The excitation energies of states observed in ^{130}Te are indicated. The inset shows the group of states which resonate strongly at this energy and which are subsequently identified as neutron particle-hole states.

$d_{3/2}$ IAR are shown in Fig. 4. The 2.731- and 2.505-MeV states do not indicate resonant behavior. However, the remaining levels from 2.268 to 2.674 MeV exhibit large on- to off-resonance yield ratios. On the basis of their resonant behavior and their excitation energies we identify these states as neutron particle-hole states with the particle in the $d_{3/2}$ shell above the ^{130}Te Fermi surface, and holes from the $d_{3/2}$ and $s_{1/2}$ subshells. The positions of the elastic scattering peaks for ^{130}Te, ^{16}O, and ^{12}C, as well as the inelastic proton peak from the 4.433-MeV state of ^{12}C, serve to span the energy region of interest and are easily identifiable in all the spectra. These were used in a least-squares calibration for the identification and determination of the excitation energy of the ^{130}Te levels. The deviations of the energies of these levels at the various angles at which they were identified, is for the most part, well within ±10 keV. The excitation energies shown in the spectra are the average energies determined by application of the above method to each angle.

A typical spectrum taken at the $s_{1/2}$ IAR is shown in Fig. 5. We expect neutron particle-hole states, with the particle in the $s_{1/2}$ shell above the ^{130}Te Fermi surface, and with the hole in the $d_{3/2}$ or $s_{1/2}$ subshells, to have excitation energies between 2.8 and 3.0 MeV. It is clear that no such states are visible in the spectra. It should be pointed out, however, that not only does the $s_{1/2}$ IAR have a much lower spectroscopic factor than that of the $d_{3/2}$ IAR, but also that the experimental measurements at the $s_{1/2}$ IAR were carried out for only one half of the total charge accumulation used at the $d_{3/2}$ IAR. Thus, it is possible that the sensitivity of the experimental measurements was not sufficient to observe states of a neutron particle-hole character at the $s_{1/2}$ IAR.

A typical spectrum at the $f_{7/2}$ IAR is shown in Fig. 6. The levels from 4.366 to 4.496 MeV, which are identified as the neutron particle-hole states, are shown on a larger scale in the inset. A total of 35 levels in ^{130}Te have been identified from the spectra at the $f_{7/2}$ IAR. These are shown in Fig. 7. Again, the elastic scattering peaks and the ^{12}C-(p,p') peak at 4.433 MeV are easily identifiable in all of the spectra, and were used in a linear least-squares calibration for the identification and determination of the excitation energy of the ^{130}Te levels.

A typical spectrum taken at the $p_{3/2}$ IAR at 10.500 MeV is shown in Fig. 8. The spectrum shows a group of many states which resonate at 10.500 MeV and which are spread over more than 1 MeV in excitation. The ^{130}Te $p_{3/2}$ spectrum is rather similar to those taken for the $N = 82$ nuclei,[15] being characterized by two closely spaced states with yields several times greater than those of the other resonating states. The centroid energies of the resonating levels are consistent with the particle-hole interpretation, and thus we tentatively identify these states as neutron particle-hole states, with the particle in the $p_{3/2}$ shell and the holes again in the $s_{1/2}$ and $d_{3/2}$ subshells. Approximately 25 states have been identified as resonating at this energy and are shown on a larger scale in Fig. 9.

D. Angular Distribution and Fits

The angular distributions were analyzed using the following expression for the scattering of protons from spin-zero targets[8,16]:

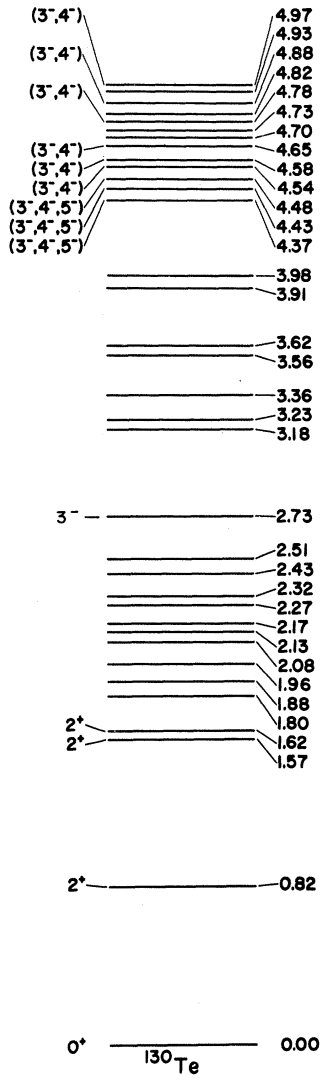

FIG. 7. An energy-level diagram for states of ^{130}Te observed at the $f_{7/2}$ IAR at 10.209 MeV in this work. The spin assignments for the 1.57- and 1.62-MeV states are from Ref. 9, whereas those in parentheses are tentative spin assignments from this work.

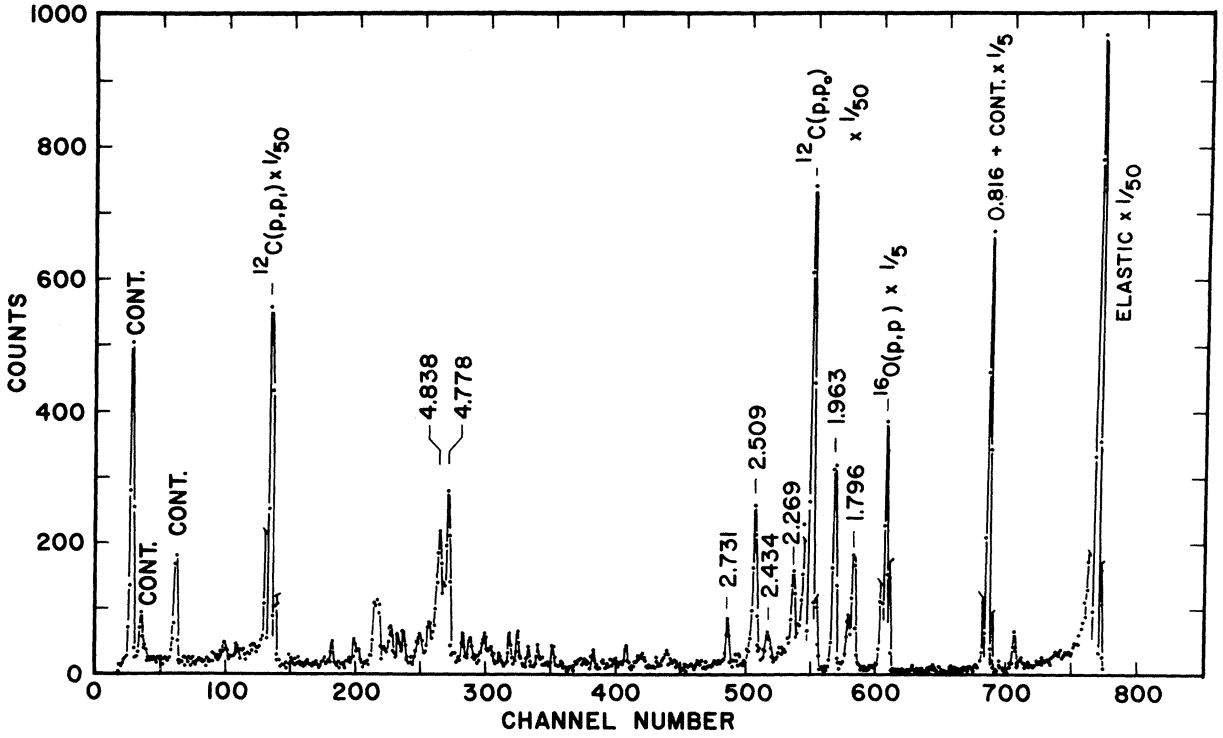

FIG. 8. Pulse-height spectrum for the inelastic scattering of protons from ^{130}Te at a scattering angle of 120° and a laboratory proton energy of 10.580 MeV which corresponds to the $p_{3/2}$ IAR at 10.500 MeV. The excitation energies indicated are for states observed in ^{130}Te.

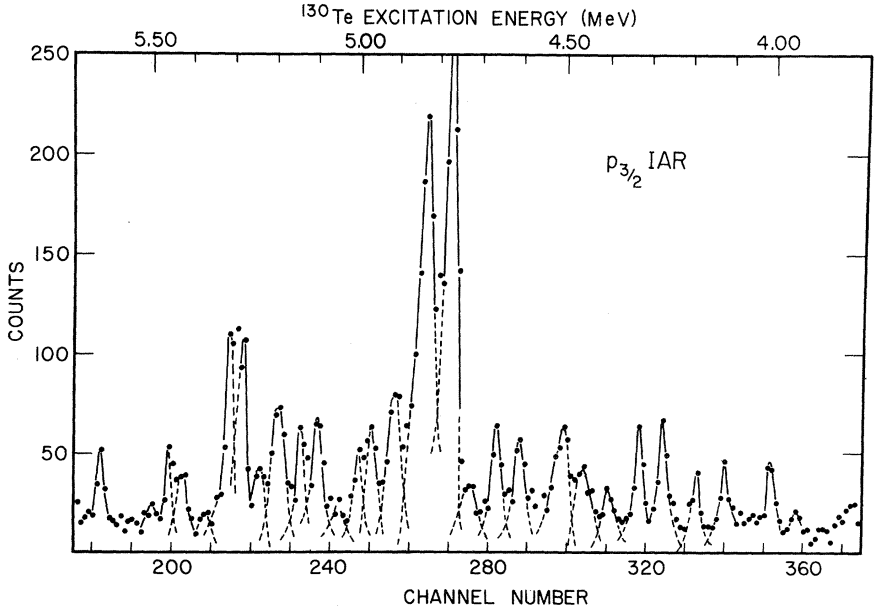

FIG. 9. Enlargement of a section of the pulse-height spectrum of Fig. 8 showing the widely spaced group of states resonating at this energy. The corresponding excitation energy for states in ^{130}Te is also shown along the top of the figure.

$$\sigma(\theta) = \frac{\lambda^2 \tilde{\Gamma}_p}{2} \frac{(2J+1)(-)^{2J-1}2^{2J-1}}{4(E-E_R)^2+\Gamma^2} \sum_{\lambda=0} P_\lambda(\cos\theta)\bar{Z}(LJLJ;\tfrac{1}{2}\lambda)$$
$$\times \sum_{j_1 j_2} \cos(\xi_{j_1} - \xi_{j_2})(\pm\tilde{\Gamma}_{Ij_1J}{}^{1/2})(\pm\tilde{\Gamma}_{Ij_2J}{}^{1/2})$$
$$\times \bar{Z}(l_1 j_1 l_2 j_2;\tfrac{1}{2}\lambda) W(j_1 J j_2 J; I\lambda) .$$

E_R, $\tilde{\Gamma}_p$, Γ, J, and L are, respectively, the resonant energy, proton elastic partial width, total width, spin, and orbital angular momentum of the analog state as obtained from the fits to the elastic scattering data. The spin and orbital angular momentum of a given hole state are j_1 and l_i, respectively, while I is the spin of the residual nucleus. The only free parameters are the inelastic proton partial widths $\tilde{\Gamma}_{IjJ}$. Using the above formula, theoretical cross sections were evaluated for a particular final-state spin using the University of Texas CDC 6600 computer. The results and the data were both displayed on an oscilloscope console from which new values of Γ_{IjJ} could be entered from a keyboard. The best fits were determined by inspection, and for final adjustment of parameters, the χ^2 values were minimized.

The states we shall discuss are expected to have configurations in which the particle is in a level above $N = 78$ ($2d_{3/2}$, $3s_{1/2}$, $2f_{7/2}$, $3p_{3/2}$), and the hole

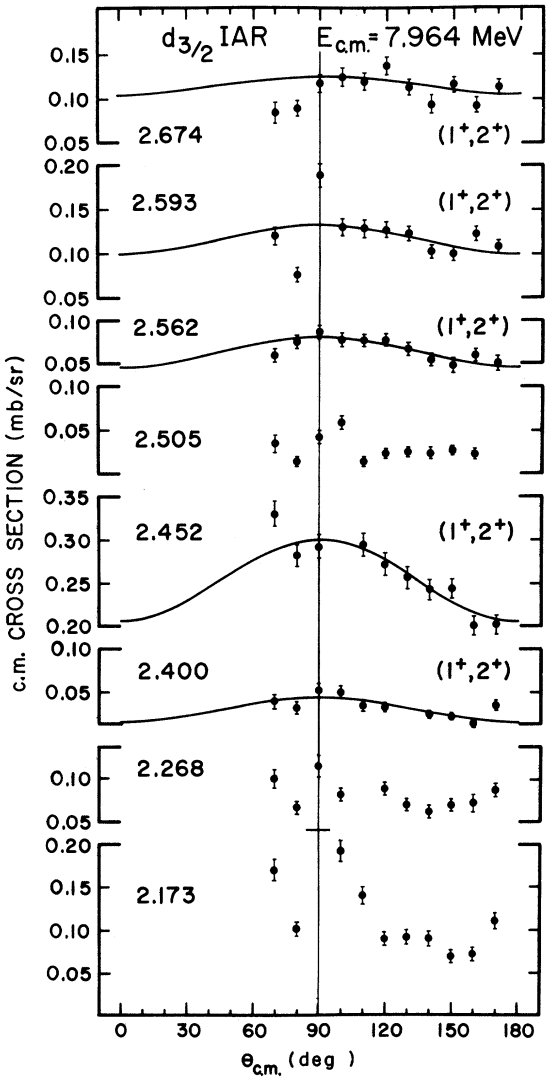

FIG. 10. Angular distributions for a group of states in ^{130}Te appearing at the $d_{3/2}$ IAR at 7.978 MeV. Fits and tentative spin assignments are shown for the five states which have been identified as neutron particle-hole states at this resonance. The excitation energies are indicated for each state.

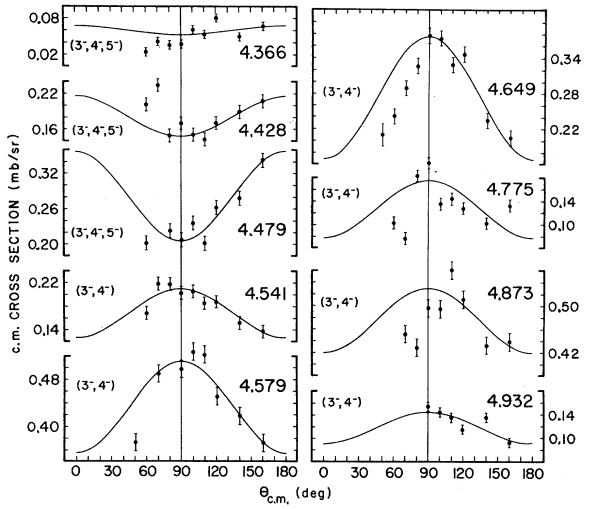

FIG. 11. Angular distributions and fits for nine of the group of states in ^{130}Te resonating strongly at the $f_{7/2}$ IAR at 10.209 MeV, and identified as neutron particle-hole states. The excitation energies in MeV and possible spin assignments are indicated for each state.

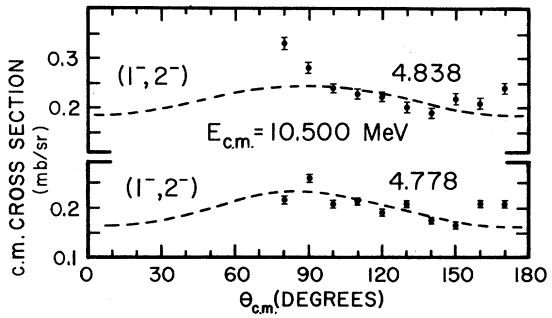

FIG. 12. Angular distributions and fits for the two strongest among a widely spaced group of many states in ^{130}Te resonating strongly at the $p_{3/2}$ IAR at 10.500 MeV and identified as neutron particle-hole states. The fits are shown as dotted lines to indicate the inclusion of the largest possible $d_{3/2}$ decay width still consistent with the data. The excitation energies in MeV and possible spin assignments are shown for each.

is in a level below the ^{130}Te Fermi surface ($2d_{3/2}$, $1h_{11/2}$, $3s_{1/2}$, $2d_{5/2}$). The possibility of $h_{11/2}$ hole states will be ignored in the present analysis because of the high angular momentum barrier involved in $h_{11/2}$ decay. Since the $d_{5/2}$ hole state is almost an MeV from the Fermi surface in ^{130}Te, it is also ignored. Particle-hole states will therefore be considered to be populated through the decay of the analog state by inelastic emission of a $d_{3/2}$ or $s_{1/2}$ proton.

The use of the above expression assumes that we may ignore the direct contributions to the inelastic cross section. Since the ratio of on-resonance to off-resonance yields at backward angles is greater than 10/1, this is not unreasonable, and we thus confine our fits to angles of 90° or greater. We also neglect interference effects between the direct and compound inelastic scattering amplitudes, since no method for treating the problem is yet available to us. These assumptions have allowed reasonable results in the application of this method of analysis to particle-hole states in ^{136}Xe.[8]

Fits were undertaken for each state for all possible values of the final-state spin. As shown in previous work,[8] only a few values of the final spin lead to unique theoretical angular distributions. Thus the analysis serves only to eliminate certain possible spin values and does not allow the unambiguous determination of the final spin for any of the states investigated.

Experimental angular distributions at the $d_{3/2}$ IAR for a group of eight states in ^{130}Te ranging from 2.1 to 2.7 MeV in excitation are given in Fig. 10. Fits are shown for the 2.400- 2.452-, 2.562-, 2.593-, and 2.674-MeV states. Theoretical fits and experimental angular distributions for 9 of the 13 resolved particle-hole states at the $f_{7/2}$ IAR are shown in Fig. 11. At the $p_{3/2}$ IAR, because of the presence of a large number of closely spaced states with rather low yields, only the two strongest states at excitations of 4.778 and 4.838 MeV were analyzed. The angular distributions and fits are presented in Fig. 12.

Figure 13 shows angular distributions for states between 2.7 and 4.0 MeV at the $f_{7/2}$ IAR. Although these states resonate at the $f_{7/2}$ IAR, they do not have excitation energies in the region expected for particle-hole states and consequently are not analyzed. It is believed that some of these states are collective in nature; in particular, the 2.731-MeV state has been previously identified from 16-MeV inelastic proton scattering investigations[17] as the 3^- octupole state. Angular distributions for the 2.505-, 2.226-, and 2.173-MeV states at the $d_{3/2}$ IAR are shown also in Fig. 10 but were not analyzed, since they appear also at the $f_{7/2}$ and $p_{3/2}$ IAR. Although neutron particle-hole states may have particle configuration admixtures, they are

TABLE V. Excitation energies, partial decay widths, and spectroscopic factors for proton inelastic scattering through the $d_{3/2}$ IAR in ^{131}I at 7.978 MeV to neutron particle-hole states in ^{130}Te. Final-state spins shown are those for which essentially identical fits were obtained. The $\frac{1}{2}$ and $\frac{3}{2}$ refer to decay of the IAR by $s_{1/2}$ and $d_{3/2}$ protons, respectively. The deduced final-state neutron particle-hole configurations are indicated in the last column. d^{-1} and s^{-1} are used to indicate respective $d_{3/2}$ or $s_{1/2}$ holes. Parentheses indicate small hole configuration admixtures.

E^* (MeV)	I^π	$\tilde{\Gamma}_{1/2\,J}$ (keV)	$\tilde{\Gamma}_{3/2\,J}$ (keV)	$S_{pp'}(\frac{1}{2})$	$S_{pp'}(\frac{3}{2})$	Configuration
2.400	1^+	0.200	0.200	0.16	0.28	$(ds^{-1})+dd^{-1}$
	2^+	0.200	0.150	0.03	0.12	$(ds^{-1})+dd^{-1}$
2.452	1^+	3.000	0.150	0.84	0.22	$ds^{-1}+(dd^{-1})$
	2^+	2.700	0.400	0.45	0.36	$ds^{-1}+(dd^{-1})$
2.562	1^+	0.725	0.125	0.24	0.22	$ds^{-1}+dd^{-1}$
	2^+	0.675	0.125	0.14	0.14	$ds^{-1}+dd^{-1}$
2.593	1^+	1.400	0.030	0.48	0.06	$ds^{-1}+(dd^{-1})$
	2^+	1.300	0.100	0.27	0.11	$ds^{-1}+(dd^{-1})$
2.674	1^+	1.375	0.018	0.53	0.03	$ds^{-1}+(dd^{-1})$
	2^+	1.200	0.100	0.28	0.13	$ds^{-1}+(dd^{-1})$

TABLE VI. Excitation energies, partial decay widths, and spectroscopic factors for proton inelastic scattering through the $f_{7/2}$ IAR in ^{131}I at 10.209 MeV to neutron particle-hole states in ^{130}Te. The deduced final-state neutron particle-hole configurations are indicated in the last column. d^{-1} and s^{-1} are used to indicate respective $d_{3/2}$ or $s_{1/2}$ holes. Parentheses indicate small hole configuration admixtures.

E^* (MeV)	I^π	$\tilde{\Gamma}_{1/2\,J}$ (keV)	$\tilde{\Gamma}_{3/2\,J}$ (keV)	$S_{pp'}(\frac{1}{2})$	$S_{pp'}(\frac{3}{2})$	Configuration
4.366	3^-	0.217	0.0035	0.035	0.028	$fs^{-1}+fd^{-1}$
	4^-	0.194	0.023	0.023	0.015	$fs^{-1}+fd^{-1}$
	5^-		0.205		0.107	fd^{-1}
4.428	3^-	0.599	0.041	0.102	0.036	$fs^{-1}+fd^{-1}$
	4^-	0.564	0.082	0.075	0.056	$fs^{-1}+fd^{-1}$
	5^-		0.640		0.360	fd^{-1}
4.479	3^-	0.787	0.176	0.143	0.168	$fs^{-1}+fd^{-1}$
	4^-	0.763	0.176	0.109	0.130	$fs^{-1}+fd^{-1}$
	5^-		0.957		0.580	fd^{-1}
4.541	3^-	0.0023	0.681	0.0003	0.708	$(fs^{-1})+fd^{-1}$
	4^-	0.616	0.070	0.095	0.058	$fs^{-1}+fd^{-1}$
4.579	3^-	1.644	0.070	0.342	0.077	$fs^{-1}+(fd^{-1})$
	4^-	1.614	0.106	0.262	0.090	$fs^{-1}+(fd^{-1})$
4.649	3^-	0.974	0.176	0.222	0.216	$fs^{-1}+fd^{-1}$
	4^-	0.047	1.115	0.008	1.062	$(fs^{-1})+fd^{-1}$
4.775	3^-	0.423	0.082	0.115	0.122	$fs^{-1}+fd^{-1}$
	4^-	0.018	0.517	0.0035	0.599	$(fs^{-1})+fd^{-1}$
4.873	3^-	1.820	0.029	0.569	0.050	$fs^{-1}+(fd^{-1})$
	4^-	1.796	0.053	0.438	0.072	$fs^{-1}+(fd^{-1})$
4.932	3^-	0.446	0.035	0.153	0.068	$fs^{-1}+(fd^{-1})$
	4^-	0.458	0.041	0.122	0.061	$fs^{-1}+(fd^{-1})$

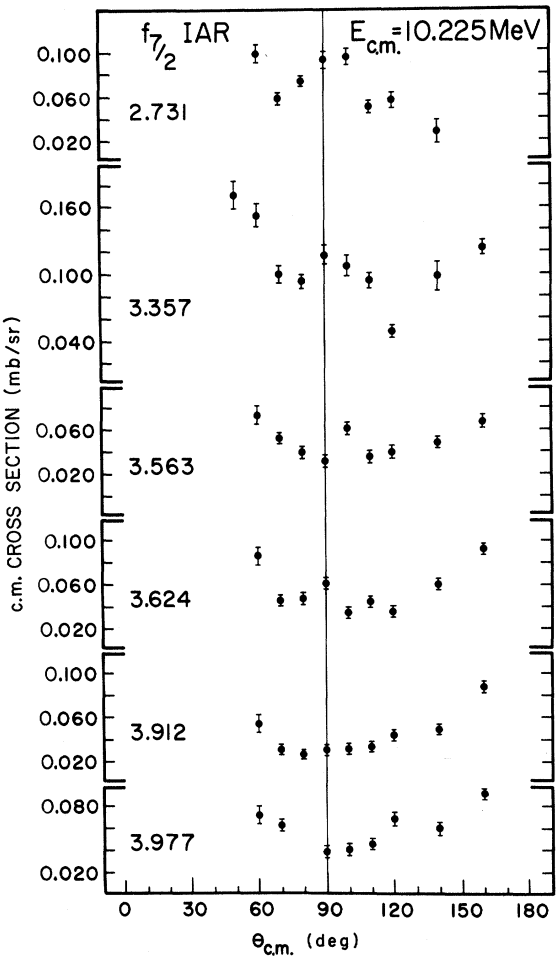

FIG. 13. Angular distributions for several additional states in ^{130}Te, some of which also resonate at the $f_{7/2}$ IAR at 10.209 MeV but are not consistent with the interpretation as neutron particle-hole states. Excitation energies are shown for each and no fits have been attempted.

TABLE VII. Excitation energies, partial decay widths, and spectroscopic factors for proton inelastic scattering through the $p_{3/2}$ IAR in ^{131}I at 10.500 MeV to neutron particle-hole states in ^{130}Te. The deduced final-state neutron particle-hole configurations are indicated in the last column. d^{-1} and s^{-1} are used to indicate respective $d_{3/2}$ or $s_{1/2}$ holes. The $d_{3/2}$ partial widths and spectroscopic factors are upper limits and are shown in parentheses. Small hole configuration admixtures are also included in parentheses.

E^* (MeV)	I^π	$\tilde{\Gamma}_{1/2\,J}$ (keV)	$\tilde{\Gamma}_{3/2\,J}$ (keV)	$S_{pp'}(\frac{1}{2})$	$S_{pp'}(\frac{3}{2})$	Configuration
4.778	1^-	1.200	(0.040)	0.27	(0.04)	$ps^{-1}+(pd^{-1})$
	2^-	1.150	(0.100)	0.15	(0.07)	$ps^{-1}+(pd^{-1})$
4.838	1^-	1.350	(0.025)	0.33	(0.03)	$ps^{-1}+(pd^{-1})$
	2^-	1.300	(0.080)	0.19	(0.06)	$ps^{-1}+(pd^{-1})$

expected only for like-parity resonances.

E. Spectroscopic Factors

Following the method of Ref. 8, spectroscopic factors were calculated from the expression

$$S_{pp'}(j)=S_{I\,jJ}=\frac{2J+1}{2I+1}\,\frac{\tilde{\Gamma}_{IjJ}}{\tilde{\Gamma}^{(sp)}_{IjJ}}$$

by first estimating the single-particle widths $\Gamma^{(sp)}_{IjJ}$ corresponding to the observed transitions. These were determined (approximately) by using the expression for the elastic proton partial width of the isobaric analog of a single-neutron state of spin j and orbital angular momentum l lying below the observed analog state by an energy equal to the excitation energy of the final state. Here $\tilde{\Gamma}^{(sp)}_{IjJ}$ were essentially the same as the $\Gamma^{(sp)}_{IjJ}$, since $f\cong 1$ at these excitation energies.

Tables V–VII list the inferred final spins, partial widths, and spectroscopic factors resulting from the application of the above analysis to the particle-hole states observed at the $d_{3/2}$, $f_{7/2}$, and $p_{3/2}$ IAR. Although the analysis limited the possible spin values for each state to those indicated in the tables, essentially identical fits were obtained for a given state for those spin values listed.

The sums of the $d_{3/2}$ and $s_{1/2}$ spectroscopic factors should account for the fullness of the $d_{3/2}$ and $s_{1/2}$ subshells, i.e.,

$$\sum S_{pp'}(j)=V_j^2(2j+1)\,,\quad \text{where } j=d_{3/2} \text{ or } s_{1/2}\,.$$

From the (d, t) measurements,[13] values for the fullness of the $d_{3/2}$ subshell, $V_j^2(3/2)=0.73$, and for the $s_{1/2}$ subshell, $V_j^2(1/2)=0.65$, were previously obtained.

At the $d_{3/2}$ IAR the $\sum S_{pp'}(3/2)$ and $\sum S_{pp'}(1/2)$ values depend somewhat on the choices for the spins of the states. Simultaneous assignment of 1^+ for all the states would more than exhaust the $s_{1/2}{}^{-1}$ strength and is not believed to be reasonable. However, no combination of spins allows the $d_{3/2}{}^{-1}$ strength to be more than about one-half accounted for. Since states with 0^+ and 3^+ final spins, which would arise from a pure $d_{3/2}\otimes d_{3/2}{}^{-1}$ configuration, were not observed in this group of states, it is reasonable that not all of the $d_{3/2}$ strength is accounted for.

At the $f_{7/2}$ IAR, the $\sum S_{pp'}(1/2)$ and $\sum S_{pp'}(3/2)$ values depend rather strongly on the spin assignments for the 4.541-, 4.649-, and 4.775-MeV states. The results for the remaining states change very little with the possible spin assignment chosen. It was not possible to satisfy fully both the expected $s_{1/2}$ and $d_{3/2}$ strengths with any assumed spin values. Since no state could be fit with a shape consistent with a 2^- assignment, it is again to be expected that the sum rule for the

$d_{3/2}$ strength is not satisfied.

The two strong states at 4.778 and 4.838 MeV analyzed at the $p_{3/2}$ IAR contain a predominant $p_{3/2} \otimes s_{1/2}^{-1}$ admixture, and exhaust about $\frac{1}{4}$ of the total $s_{1/2}^{-1}$ strength. The fits to these angular distributions were generated so as to include the largest $d_{3/2}$ decay width consistent with a reasonable fit, and are shown in Fig. 13 as dotted lines. For this reason, the resulting $d_{3/2}^{-1}$ spectroscopic factors are to be interpreted as upper limits and are included in Table VI in parentheses.

The analyses at the $d_{3/2}$, $f_{7/2}$, and $p_{3/2}$ IAR indicate several features. In all cases the stronger states contain predominant $J \otimes s_{1/2}^{-1}$ admixtures, and we conclude that the $s_{1/2}^{-1}$ strength can be essentially accounted for. On the other hand there is a conspicuous absence of all but a very few states with strong $d_{3/2}^{-1}$ admixtures. Further, those admixtures detected account for at most only about half of the expected $d_{3/2}^{-1}$ strength. It may be seen from the expression used in this analysis that the coherent admixing of the different hole configurations gives rise to interference terms in the resulting cross sections. It is precisely these interference effects which allow the small $d_{3/2}^{-1}$ admixtures to be detected. The cross section arising from a pure $J \otimes d_{3/2}^{-1}$ configuration is expected to be smaller than that for the $J \otimes s_{1/2}^{-1}$ on the basis of penetrability considerations. Since such cross sections contain no interference terms, states with the former configuration are rather difficult to observe. Consequently, the $d_{3/2}$ decay is best observed as an admixture in states containing appreciable $J \otimes s_{1/2}^{-1}$ configurations.

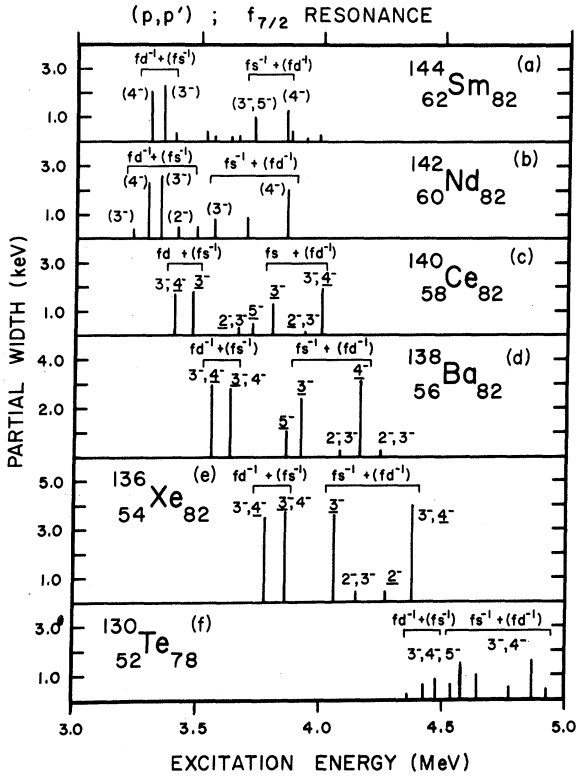

FIG. 14. Total inelastic partial widths for proton decay of the $f_{7/2}$ IAR to neutron particle-hole states in the nuclei shown. The predominant configurations are indicated by brackets, where the f stands for an $f_{7/2}$ neutron coupled with $d_{3/2}$ and $s_{1/2}$ neutron holes, represented by d^{-1} and s^{-1}, respectively. The spins shown are those consistent with the geometry and fits to the data, where available, and the underlined values are the assignments of the various authors. The sources for these results are (a) Ref. 18, (b) Ref. 5, (c) Ref. 6, (d) Ref. 7, (e) Ref. 8, (f) Ref. 14, and this work.

F. Comparison with $N = 82$ Isotones

A comparison of the partial widths for the proton decay of the particle-hole states at the $f_{7/2}$ IAR in ^{130}Te with those in the $N = 82$ isotones ^{136}Xe, ^{138}Ba, ^{140}Ce, ^{142}Nd, and ^{144}Sm[18] is shown in Fig. 14. The diagram is similar to one presented by Morrison for the $N = 82$ isotones.[19] The partial width for each state in which admixtures are present is graphed as the sum of the $d_{3/2}$ and $s_{1/2}$ partial widths, the sum being independent of the final-state spin. For many states, the same fit could be obtained for more than one final-state spin, and the underlined values represent the choices of the respective authors. The results for ^{130}Te are very similar to those for the $N = 82$ isotones. In all cases the particle-hole states fall into two main groups. The groups lying higher in excitation are the result of predominant $s_{1/2}$ decay, and those at lower excitation, from $d_{3/2}$ decay. The centroids of the $d_{3/2}$ and $s_{1/2}$ decay strengths are consistent with those calculated from the binding energies of the $d_{3/2}$ and $s_{1/2}$ neutron holes and the $f_{7/2}$ particle, as determined from respective (d, t) and (d, p) measurements.

Since the $f_{7/2}$ IAR in ^{130}Te has a smaller spectroscopic factor than those of the $N = 82$ isotones, and since the $s_{1/2}$ and $d_{3/2}$ subshells in ^{130}Te are not full, one expects and observes that the inelastic widths for particle-hole states in ^{130}Te are approximately a factor of 2 less than the corresponding widths for the $N = 82$ isotones. Fractionization in ^{130}Te is more pronounced, since it is four neutrons away from the closed neutron shell at $N = 82$.

Except for the two states at 4.778 and 4.838 MeV, the high density of particle-hole states at the $p_{3/2}$ IAR makes a realistic analysis of the data impossible with the present experimental resolution. At these energies direct excitation of these states is quite low and they disappear into the background a few hundred keV off resonance. Consequently,

it is not possible to deduce reliably from the data which states at the $p_{3/2}$ IAR also correspond to states appearing at the $f_{7/2}$ IAR. Although the excitation energies are approximately the same for the 4.775-MeV state at the $f_{7/2}$ IAR and the 4.778-MeV state at the $p_{3/2}$ IAR, the final-state spins consistent with a good fit to the data (3^- or 4^- at the $f_{7/2}$ IAR and 1^- or 2^- at the $p_{3/2}$ IAR) indicate that these are not identical states. In the case of the $N = 82$ nuclei, the two strong particle-hole states at the $p_{3/2}$ IAR have been assigned possible spins of 1^- or 2^-, consistent with the results of the present work.

The large number of resonant inelastic states at the $p_{3/2}$ IAR indicates that the single-neutron particle-hole picture is far from being realized. A similar situation is observed at the $p_{3/2}$ IAR in the $N = 82$ nuclei.[15] It has been shown[10] that the $p_{3/2}$ IAR parent state is well described by mixing the configuration formed by coupling an $f_{7/2}$ neutron to the 2_1^+ core with that formed from the $p_{3/2}$ neutron coupled to the 0^+ core, i.e.,

$$|\psi\rangle_{3/2^-} = \alpha\,|n_{3/2^-} \otimes C(0^+)\rangle_{3/2^-} + \beta\,|n_{7/2^-} \otimes C^*(2_1^+)\rangle_{3/2^-}\,.$$

$C(0^+)$ and $C^*(2_1^+)$ represent the respective wave functions of the ground state and the 2^+ first excited state. For the $N = 82$ nuclei, the elastic spectroscopic factor α^2 is approximately 0.3 to 0.4, and the value of β^2 is approximately 0.6 to 0.7.[10] Consequently, the $p_{3/2}$ IAR wave function should be well described by

$$T^-[\,|\psi\rangle_{3/2^-}] \rightarrow \frac{1}{(2T_0+1)^{1/2}}[\alpha\,|p_{3/2^-} \otimes C(0^+)\rangle_{3/2^-} + \beta\,|p_{7/2^-} \otimes C^*(2_1^+)\rangle_{3/2^-}]$$
$$+ \frac{(2T_0)^{1/2}}{(2T_0+1)^{1/2}}[\alpha\,|n_{3/2^-} \otimes A(0^+)\rangle_{3/2^-} + \beta\,|n_{7/2^-} \otimes A^*(2_1^+)\rangle_{3/2^-}]\,.$$

Elastic scattering results from the first term in the above expression, and inelastic proton decay to the 2_1^+ excited state from the second term. Configurations indicated by the third term decay preferentially to particle-hole states, with the particle in the $p_{3/2}$ state, and the hole in one of the subshells lying below the closed $N = 82$ shell, the $d_{3/2}$ and $s_{1/2}$ subshells being preferred from penetrability considerations. Configurations indicated by the fourth term decay preferentially to neutron particle-hole states built on an excited 2_1^+ core, with the particle in the $f_{7/2}$ state above the $N = 82$ shell.

It is possible that mixing may occur between the particle-hole states built on the ground state and those built on the 2_1^+ excited states, and that this mixing may contribute to the large number of weakly excited resonating states observed at the $p_{3/2}$ IAR in the (p,p') spectra of the $N = 82$ nuclei. $|nA^*\rangle$ states should be observed more easily in ^{130}Te than in the $N = 82$ nuclei because of the larger value of β^2 in ^{130}Te of approximately 0.8.[10] Also, the mixing of $|nA^*\rangle$ with $|nA\rangle$ states is expected to be greater in ^{130}Te than in the $N = 82$ nuclei because of the smaller spacing between the 2_1^+ state and the ground state in ^{130}Te. The centroid energies for such $|nA^*\rangle$ states in ^{130}Te should lie at an excitation energy approximately 800 keV higher than those of the $|nA\rangle$ states. The observed excitation energies of the group of resonant states span the expected excitation energies expected for both $|nA\rangle$ and $|nA^*\rangle$ particle-hole states. Consequently we conclude that we do see indirect evidence for neutron particle-hole states in ^{130}Te built on the 2_1^+ core. However, because of the large number of weakly excited and closely spaced states observed, and because of the possibility that considerable mixing of states is involved, the application of the type of analysis described in this paper is believed to be difficult and ambiguous at the $p_{3/2}$ IAR.

IV. SUMMARY

^{130}Te proton elastic scattering excitation functions from 7.8 to 12.0 MeV have been reanalyzed using the approach of Zaidi and Darmodjo to obtain energies, partial widths, and total widths of the IAR. The compound-nuclear states in ^{131}I are analogs of states in ^{131}Te formed by the addition of a neutron to the ^{130}Te core. Single-particle decay widths were calculated in the framework of the Lane model, and after correction for absorption due to the background of $T^<$ states, were used to calculate the elastic spectroscopic factors. The results for a total of 14 resonances analyzed compare favorably with those of the other elastic analyses and with the (d,p) investigations.

Excitation energies of 42 states in ^{130}Te were determined from the spectra taken at the various IAR. The resonant behavior of three groups of states observed, respectively, in the inelastic scattering data at the $d_{3/2}$, $f_{7/2}$, and $p_{3/2}$ IAR at 7.978, 10.209, and 10.500 MeV was found to be characteristic of neutron particle-hole excited states. Fits to the on-resonance angular-distribution data for five states at the $d_{3/2}$, nine states at the $f_{7/2}$, and two states at the $p_{3/2}$ IAR have allowed us to determine inelastic partial widths, hole con-

figurations, and possible spins and parities for these states. Approximations for the single-particle partial widths again enable spectroscopic factors to be evaluated. The sums of the spectroscopic factors for $d_{3/2}$ and $s_{1/2}$ decay indicate the $s_{1/2}^{-1}$ strength to be mostly accounted for and the $d_{3/2}^{-1}$ strength to be about $\frac{1}{2}$ accounted for at these resonances.

The widely spaced group of a large number of states resonating at the $p_{3/2}$ IAR at 10.500 MeV is believed to arise from the mixing of ordinary neutron particle-hole states built on the 0^+ core with states of a similar configuration built on the 2^+ first excited state at 0.816-MeV excitation. Because of this additional complication, only the two strongest states at the $p_{3/2}$ IAR were analyzed in the framework of the present investigation.

ACKNOWLEDGMENTS

The authors are greatly indebted to Dr. W. R. Coker for stimulating comments and criticism. We also wish to thank Dr. S. A. A. Zaidi for helpful discussions.

---

†Work supported in part by the U. S. Atomic Energy Commission.

*Present address: Physics Department, Texas Christian University, Fort Worth, Texas 76129.

[1]J. L. Foster, Jr., P. J. Riley, and C. Fred Moore, Phys. Rev. 175, 1498 (1968).

[2]S. A. A. Zaidi and S. Darmodjo, Phys. Rev. Letters 19, 1446 (1967).

[3]A. Graue, E. Jastad, J. R. Lien, P. Torvund, and W. H. Moore, Nucl. Phys. A103, 209 (1967).

[4]C. D. Kavaloski, J. S. Lilley, P. Richard, and N. Stein, Phys. Rev. Letters 16, 807 (1966); C. F. Moore, J. G. Kulleck, P. von Brentano, and F. Rickey, Phys. Rev. 164, 1559 (1967); S. A. A. Zaidi, J. L. Parish, J. G. Kulleck, C. F. Moore, and P. von Brentano, *ibid.* 165, 1312 (1968); G. H. Lenz and G. M. Temmer, Nucl. Phys. A112, 625 (1968); P. Richard, N. Stein, C. D. Kavaloski, and J. S. Lilley, Phys. Rev. 171, 1308 (1968); W. R. Wharton, P. von Brentano, W. K. Dawson, and P. Richard, *ibid.* 176, 1424 (1968); J. Solf, C. F. Moore, E. Grosse, and P. von Brentano, Nucl. Phys. A139, 523 (1969); J. G. Kulleck, P. Richard, D. Burch, C. F. Moore, W. R. Wharton, and P. von Brentano, to be published.

[5]O. Dietzsch and J. L. Foster, in *Proceedings of the International Conference on Properties of Nuclear States, Montréal, Canada, 1969,* edited by M. Harvey *et al.* (Presses de l' Université de Montréal, Montréal, Canada, 1969), p. 263.

[6]A. Heusler, H. L. Harney, and J. P. Wurm, Nucl. Phys. A135, 591 (1969).

[7]G. C. Morrison, N. Williams, J. A. Nolen, Jr., and D. von Ehrenstein, Phys. Rev. Letters 19, 592 (1967).

[8]P. A. Moore, P. J. Riley, C. M. Jones, M. D. Mancusi, and J. L. Foster, Jr., Phys. Rev. Letters 22, 356 (1969).

[9]J. Burde, G. Engler, A. Ginsburg, A. A. Jaffe, A. Marinov, and L. Birstein, Nucl. Phys. A141, 375 (1970).

[10]H. R. Hiddleston and P. J. Riley, Phys. Letters 32B, 425 (1970).

[11]S. A. A. Zaidi and P. Dyer, Phys. Rev. 185, 1332 (1969).

[12]S. Darmodjo, Ph.D. dissertation, University of Texas at Austin, 1968 (unpublished).

[13]R. K. Jolly, Phys. Rev. 136, B683 (1964).

[14]H. R. Hiddleston, V. D. Mistry, C. L. Hollas, and P. J. Riley, in *Nuclear Isospin,* edited by J. D. Anderson, S. D. Bloom, J. Cerny, and Wm. W. True (Academic Press Inc., New York, 1969), p. 661.

[15]K. Mudersbach, A. Heusler, and J. P. Wurm, Nucl. Phys. A146, 477 (1970).

[16]S. A. A. Zaidi, P. von Brentano, D. Rieck, and J. P. Wurm, Phys. Letters 19, 45 (1965).

[17]W. Makofske, W. Savin, H. Ogata, and T. H. Kruse, Phys. Rev. 174, 1429 (1968).

[18]D. Spalding, O. Dietzsch, J. L. Foster, and W. C. Weitkamp, Bull. Am. Phys. Soc. 13, 659 (1968).

[19]G. C. Morrison, in *Nuclear Isospin,* edited by J. D. Anderson, S. D. Bloom, J. Cerny, and Wm. W. True (Academic Press Inc., New York, 1969), p. 460.